The origins of friction and the growth of graphene, investigated at the atomic scale

Baarle, D.W. van

Chapter 4

Computational results, their interpretation and implications

The refined 2-mass-2-spring-model, featuring a very small dynamic mass representing the tip apex, is evaluated extensively by numerical calculations. Several friction regimes were explored systematically. The most striking and elucidating results are presented in this chapter, together with their interpretation. We also highlight the implications of the results of our studies.

4.1 Results - a limited regime of atomic resolution

Following the discussion presented in Chapter 2, the friction behaviour of a friction contact is dependent on (amongst others) the number of atoms in the tip apex that make contact with the substrate, N_c, and the number of tip apex atoms that effectively move together with the contact atoms, N_d. In order to study the impact of these parameters, we performed numerical calculations in which N_c was fixed at a value of 100 (atoms) and N_d was varied from 2500 to 10^8 atoms. The value of 100 atoms for N_c is larger than the number that one should associate with a typical friction contact. The number of contacting atoms in the case of contact-AFM is typically 10. For FFM, we should expect a similar number. We have chosen a higher value for N_c in order to avoid unpractically long calculation times. However, our results should still be considered representative for the stick-slip dynamics in typical FFM experiments. The values for N_d were chosen such that, in according to Equation 2.9, overdamped, critically damped and underdamped

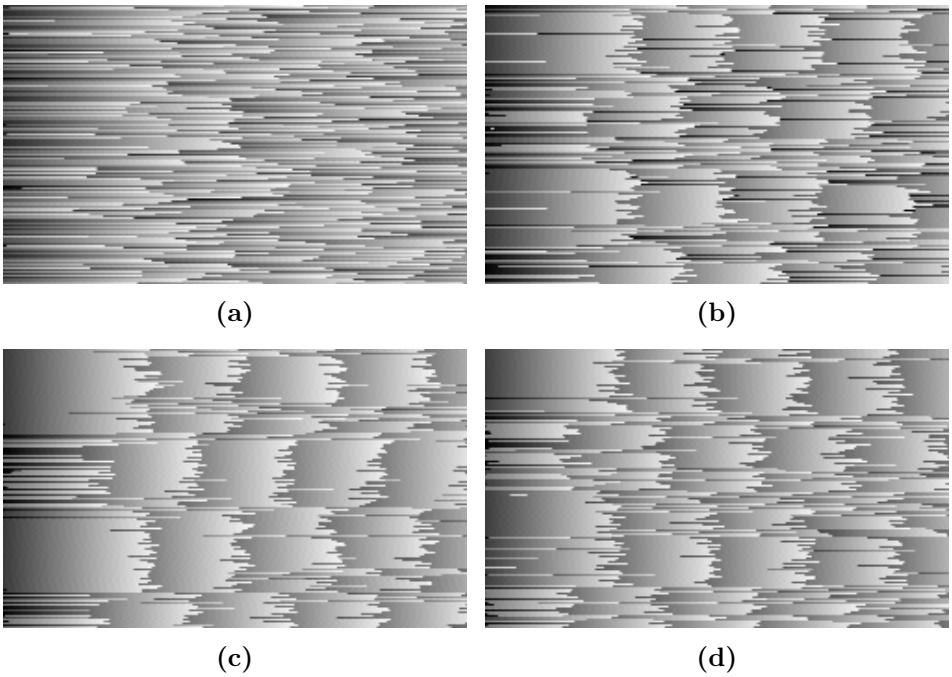

Figure 4.1: Numerically calculated lateral force maps, with the parameters chosen to match those of the FFM-experiments. ($k_{\mathrm{cant}} = 30\,\mathrm{N/m}$, $k_{\mathrm{d}} = 2\,\mathrm{N/m}$, $v_{\mathrm{supp}} = 30\,\mu\mathrm{m/sec}$, $m_{\mathrm{at}} = 74\,\mathrm{amu}$, $U_0 = 0.8\,\mathrm{eV(peak\text{-}peak)}$, $T = 298\,\mathrm{K}$), and a number of contacting atoms of $N_{\mathrm{c}} = 100$ (see text). The number of dynamic atoms N_{d} was chosen differently for each panel, in order to vary the damping regime. (a) $N_{\mathrm{d}} = 10^8$, corresponding to one-hundredfold underdamped motion. (b) $N_{\mathrm{d}} = 10^6, \widehat{=}$ tenfold underdamped. (c) $N_{\mathrm{d}} = 4 \times 10^4, \widehat{=}$ twofold underdamped. (d) $N_{\mathrm{d}} = 2500, \widehat{=}$ twofold overdamped. Note that the two underdamped cases in (a) and (b) show many occasions with multiple slip events and that the overdamped case shows an increase in the force fluctuations. For lateral force patterns with a well-defined lattice signature, the damping should be close to critical.

situations were realized. Other parameters were chosen to match typical FFM experiments. The calculations resulted in 2-dimensional lateral force maps, of which typical examples are presented in Figure 4.1.

The numerically calculated friction force maps are in agreement with the qualitative damping rate of the friction contact that can be calculated via Equation 2.8. In the regime of a critically damped tip apex (e.g. Figure 4.1c), a regular stick-slip (SS) pattern was observed, which presents itself in a clearly visible atomic periodicity and a minor amount of thermal noise, similar to what was observed in FFM experiments. As expected, all excess kinetic energy that the tip apex acquired during the slip was dissipated rapidly enough to prevent the occurrence of double slips. On the other hand, a heavily underdamped tip apex, which corresponds to Figure 4.1a, led to a nearly complete vanishing of the atomic periodicity in the friction maps. Although the SS-behaviour was still observed, the motion had become very irregular: the precise moment and the length of the slip were unpredictable. Slips with a length of more than one atomic spacing (the so-called multiple slips) occurred frequently, which indicated that the excess kinetic energy of the tip apex was not dissipated in time and the tip apex was able to overcome the next potential barrier. As a direct consequence, the tip was able to slip to the second-next potential well at once.

The result of the calculation in which the tip apex was chosen to be slightly overdamped, is shown in Figure 4.1d. A remarkable observation is the slight degradation of the atomic periodicity in the SS-behaviour. As further overdamping of the tip apex resulted in very long calculation time, no complete 2D-maps of heavily overdamped systems were calculated. However, a quick survey showed that a more overdamped friction contact destroyed the atomic periodicity even more. A close look at the manner in which the atomic periodicities were lost, revealed that it originated in a higher degree of unpredictability of the precise moment a slip was initiated. In contrast to the underdamped situation, the occurrence of multiple slips was negligible. The origin of this stochastic-type of stick-slip can be found easily in the noise term present in the Langevin equations: it is the fluctuation-dissipation theorem that is causing the noise term to increase in a situation of high dissipation. In the overdamped case, the dissipation is relatively high and so is the noise term. These fluctuations dominate the motion of the tip apex, resulting in a loss of atomic periodicity in the friction curves.

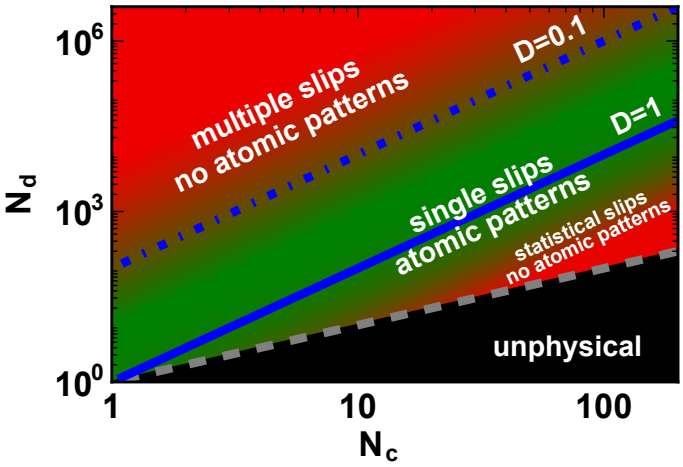

Figure 4.2: Friction 'phase' diagram as a function of the number of atoms N_c in the contact and the number of dynamic atoms N_d. The blue, solid line indicates the situation for critical damping of the tip apex motion, $D = N_c^2/N_d = 1$, the blue dash-dotted line indicates a tenfold underdamped system. The colours indicate the quality of the stick-slip patterns. Green corresponds to a clearly recognizable atomic lattice, and red to strongly washed out patterns.

4.2 Interpretation - modes of friction

Our theoretical description of the tip apex, presented in Chapter 2, already predicted friction behaviour of the tip apex that should depend on the tip geometry. The numerical calculations presented here show this dependence too. In case of a close to critically damped tip apex, regular SS-motion is observed. A deviation from the critically damped situation leads to a loss of atomic periodicity in the lateral force signal of the cantilever. Apparently, a limited window exists where the dissipation is high enough to avoid multiple slips and where the statistical fluctuations are not causing irregular slip occurrences.

This friction picture can be summarized and visualized by a 'phase' diagram as presented in Figure 4.2. This figure indicates the quality of the atomic patterns as function of the tip geometry. The colour coding is based on the numerical calculations that we performed, the indicated lines are drawn in accordance to Equations 2.8 and 2.9. We see that the friction regimes are characterized by the geometry of the tip, which is defined by N_d and N_c. The lower right, black coloured, area is physically inaccessible as the ensemble of dynamic atoms at least consist of the atoms making up

the friction contact.

In Figure 4.2, just above the unphysical area, a narrow regime is present characterised by a relatively small number of dynamic atoms and a large contact size. This makes the dissipation rate of the friction contact relatively high, resulting in overdamped behaviour. The high dissipation increases the noise on the contact behaviour, which explains that this regime is characterised by statistically initiated jumps (c.f. Figure 4.1d). The blue solid line in Figure 4.2 indicates the case of a critically damped friction contact, $D = 1$. The area around this line represents a regime in which regular SS-motion of a tip of an FFM will yield the typically observed atomic lattices in the 2D lateral force maps.

In case of a slightly underdamped tip geometry, e.g. $D = 0.1$ indicated by the dashed blue line in Figure 4.2, multiple slips occur. These slips degrade the atomic patterns in the 2D force maps, as can be seen in Figure 4.1b, where the tip geometry realized a damping factor $D = 0.1$. An even further underdamped scenario, having a damping factor of $D = 0.01$, yields a complete vanishing of atomic periodicities in the observations, see Figure 4.1a. This situation belongs to the red area in the top-left corner of the friction phase diagram shown in Figure 4.2.

4.3 Implications - tuneable friction

In view of the strict conditions on the tip geometry for obtaining atomic patterns by an FFM, visualized by the green area in the phase diagram in Figure 4.2, one might wonder why so many FFM-experiments yield regular SS-motion that results in the typically observed atomic periodicities. The answer to this question is surprisingly natural: most tips used in AFM- and FFM-experiments have geometries that make the tip apex naturally fall in the green area of the phase diagram. As a result, a typical AFM probe has a tip apex that will realise an approximately critically damped friction contact. But, on the other hand, in case we would use a completely rigid tip in an FFM, which one might regard as the optimal configuration, we would never observe regular SS-motion. Namely, this would make the dynamic mass very high, which would bring us to the upper-left, red area in the friction phase diagram: a heavily underdamped situation that destroys the observation of atomic patterns.

Our characterisation of single asperities and the narrow window of tip geometries that lead to regular SS-motion allows us to think about new strategies to control friction. For example, although the red areas in Figure 4.2 indicate a loss of regular SS, friction contacts that fall in the upper-left

red zone will result in a reduction of the average friction force experienced. The further away from the critically damped scenario, the more delocalized the single asperities will be. We regard this as a novel and attractive way to achieve low-friction contacts. Based on this approach, we can not only think of individual 'designer' asperities, combining a specific tip apex geometry and stiffness. The concept can be used on a macroscopic scale by an appropriate patterning of the entire surface into an ensemble of such low-friction contacts, thus generating a macroscopic, low-friction interface.

4.4 A detailed look at FFM experiments and their interpretation

Experimental reports that can be used to verify our theoretical work are rather scarce as highly time-resolved experiments are required. One of the most suited reports in the literature is the work performed by S. Maier et al.[15]. In their work, the focus was on fluctuations and jump dynamics in atomic friction experiments. Using a FFM equipped with a high-speed data acquisition system, single-asperity friction on graphite and KBr(100) was studied with a 20 MHz sampling rate. Here we will evaluate the experimental data reported in Reference [15] in the light of our work and based on this we present an alternative interpretation of their findings. The results obtained by our numerical calculations will be used to study and discuss both the tip apex behaviour and the impact of this behaviour on the observed lateral deflection of the cantilever. Consequently, the validity and strength of our numerical approach will emerge.

4.4.1 Data averaging

Both in numerical calculations and in experiments, the acquired data is often averaged in order to cancel high-frequency noise. Extra attention has to be paid in case the data rate after averaging is approaching the frequency of relevant components in the original signal within one order of magnitude. The impact of data averaging on the amplitudes of harmonics in the original signal can be evaluated by calculating the transfer function of such a digital process. In our case, data averaging of a sine function $f_0(t) = A\sin(\omega_0 t)$ over a certain time interval T_{ave} can be described mathematically as follows:

$$\langle f_0(t)\rangle_{T_{\text{ave}}} = \frac{1}{T_{\text{ave}}}\int_{t-T_{\text{ave}}/2}^{t+T_{\text{ave}}/2} f_0(t')dt'. \tag{4.1}$$

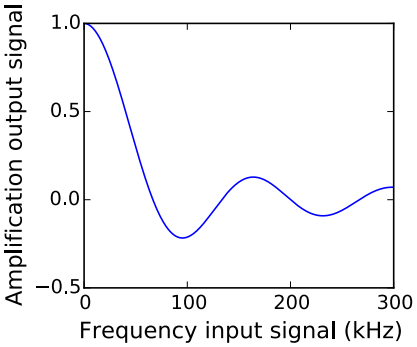

Figure 4.3: Transfer function of typical digital data averaging of an input signal towards a 66 kHz sampling rate as function of the input frequency. The graph shows that even at a frequency as high as 300 kHz signals are not completely suppressed by the low sampling rate and that at intermediate frequencies the undersampling can even lead to sign reversals of the filtered signal.

For simplicity, we show the operation in continuum space. Performing the integration and using the product-to-sum identities, leads to

$$\langle f_0(t)\rangle_{T_{\text{ave}}} = \frac{2}{\omega_0 T_{\text{ave}}} f_0(t) \sin\left(\frac{1}{2}\omega_0 T_{\text{ave}}\right), \tag{4.2}$$

which can be rewritten into

$$\langle f_0(t)\rangle_{T_{\text{ave}}} = f_0(t)\text{sinc}\left(\frac{1}{2}\omega_0 T_{\text{ave}}\right). \tag{4.3}$$

This means that data averaging over a time interval T_{ave} affects the amplitude of a harmonic with frequency ω_0 with a factor $\text{sinc}\,(0.5\omega_0 T_{\text{ave}})$.

In case of a 15 μs time resolution (as used in the work in Reference [15], which was the result of averaging over 50 data points of data recorded with 3.3 MHz sampling frequency), the transfer function of the data averaging applied in their situation is plotted in Figure 4.3. This figure shows the ratio between the output and input amplitudes of a harmonic signal, as function of the frequency of the harmonics in the input signal.

In order to let the calculations performed in our work match with the work done in Reference [15], we configured our filtering such that it matched with the filtering performed in Reference [15] as closely as possible. Since the eigenfrequency of the modelled cantilever was not precisely identical to that of the cantilever in the experiment, we adjusted the filter frequency

accordingly. In practice, the data for the modelled cantilever (which was stored to a file with a sampling rate of 20 MHz) was averaged over 600 data points.

As a side remark, we note that the impact of data averaging on thermal noise is such that the high-frequency part of the noise (roughly > 0.5 MHz) is removed completely and hence the observed noise band is reduced.

The residual noise band Maier et al. observed after data averaging, had an amplitude of 0.7 nN. The primary origin of this noise cannot be thermal fluctuations, as a quick calculation shows that unfiltered thermal noise on the cantilever would result in a noise force with an amplitude less than 0.3 nN. Additional data averaging would reduce this amplitude even further by nearly one order of magnitude. Hence we assume that the noise band reported in Reference [15] has its major origin in electronic noise generated by the photodiode.

4.4.2 A close look at the motion of the tip apex

The calculations performed in our studies take into account the full dynamics of both the cantilever and the tip. This detailed study allows us to zoom in on the motion of the tip apex and on the occurrences op slips and allows us to follow the reaction of the cantilever.

In order to compare the cantilever behaviour and the tip apex dynamics, one has to bridge a gap of timescales (kHz vs THz). For this, histograms were made of the tip apex positions. Every single calculation cycle (THz-scale), the x- and y-coordinates of the tip apex were stored internally. Then (on the MHz-scale) a histogram was constructed out of all tip-apex-position-data-points. This histogram was written to a file. After the calculations were finished, a Python-script imported all these histograms and plotted them as function of time (e.g. see the upper panel of Figure 4.4). In this way, a 2-dimensional map was created, which clearly shows the most frequently occurring tip apex positions along a single direction (e.g. x), over time. These maps, plotted together with the lateral force on the cantilever, enable us to look at the origin of the typically measured friction traces and to analyse the interplay between tip apex and cantilever.

A typical example of this interplay is shown in Figure 4.4. This figure is based on a simulation in which a tip was scanning a graphite lattice. In the upper panel, a histograms of the x-coordinate of the tip apex position is shown as function of time. Each individual histogram is plotted along the vertical axis and shows a distribution of the x-positions of the tip apex during a certain time interval. This map shows that the tip has performed effectively four slips during the calculations. However, an accurate look at

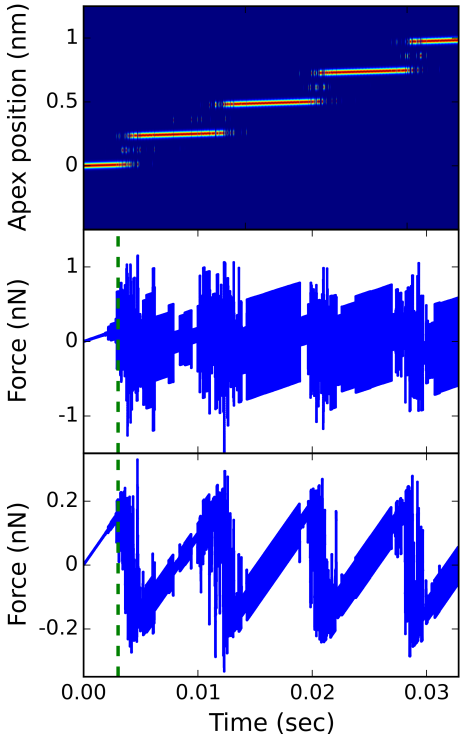

Figure 4.4: (Upper panel) Statistical representation of the x-coordinate of the tip-apex plotted as function of time. Each vertical column of pixels originates from one histogram. The colours run from blue (zero probability) via yellow (intermediate) to red (maximum probability). (Center panel) Unfiltered, 20 MHz data representing the lateral force on the cantilever. (Bottom panel) Lateral force data, originating from the cantilever, averaged in order to the simulate experimental conditions in Reference [15], as detailed in the text. A zoom in of the data at the position that is indicated by the green, dashed line is presented in Figure 4.5. The calculation was performed on a graphite lattice, using the following parameters: $U_0 = 0.45\,\mathrm{eV_{pp}}$, $m_{\mathrm{cant}} = 10^{-10}\,\mathrm{kg}$, $m_{\mathrm{d}} = 10^{-20}\,\mathrm{kg}$, $v_{\mathrm{supp}} = 30\,\mathrm{nm/sec}$, and $T = 298\,\mathrm{K}$.

each of these four slip events reveals that at each slip the tip apex jumps multiple times at high frequency forward and backward from one lattice well to the next.

The second panel presented in Figure 4.4 shows the lateral force on the cantilever. The data sampling rate was 20 MHz. The third panel also presents the lateral force on the cantilever, but in this panel the data points were averaged over 600 points in order to effectively create the same conditions as realized in the experiments in Reference [15]. The impact of data averaging is clearly visible from the difference between the lower two panels of Figure 4.4: the SS-signature is much more pronounced after data averaging. The effect of data averaging is identical to the one reported in Reference [15]. Our focus on the tip apex position in combination with the force on the cantilever forms an additional tool that allows us to study the interaction between the tip and cantilever in more detail using our calculation model.

The next sections focus on the interpretation of the dynamics of both the cantilever and the tip apex. The experimentally inaccessible timescale, at which the tip apex moves, will be accessed by our calculations. Based on the experimental support of the results of our calculations, we reveal the behaviour of the apex of a friction contact.

4.4.3 Cantilever oscillation

The impact of a single slip-event of the tip apex on the cantilever can be studied when we compare the non-averaged (20 MHz) lateral-force data of the cantilever with the history of the tip apex position. In Figure 4.5, a zoom-in is presented of the first part of the first slip-event shown in Figure 4.4. The upper panel shows that the tip apex jumps forward and backward between lattice wells multiple times at a high frequency. The influence of each slip event of the tip apex on the cantilever is visible in the lower panel of Figure 4.5. In this figure we see that the lateral force on the cantilever oscillates. The force oscillation occurs with the cantilever eigenfrequency and is a direct consequence of the oscillatory motion of the cantilever. The amplitude and phase of the cantilever oscillation are both changed abruptly each time that the tip apex jumps.

A comparison of the middle and bottom panels of Figure 4.4 with the bottom panel of Figure 4.5 enables us to explain the complex motion of the cantilever in Figure 4.4. Especially the middle panel in Figure 4.4 shows a noisy, scattered set of data points during episodes where the tip apex jumps forward and backward many times between its current and its next lattice position. The abrupt changes in the amplitude and phase of the

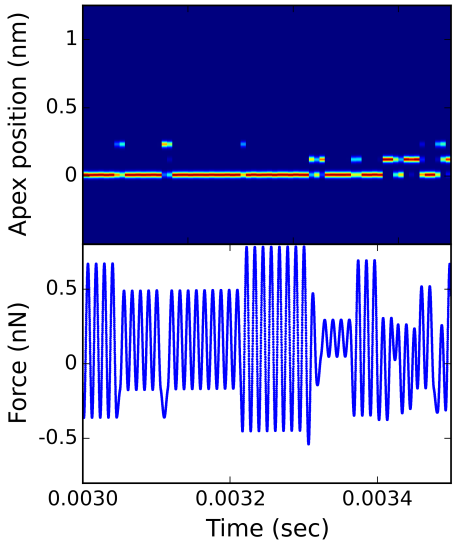

Figure 4.5: Zoom in of Figure 4.4 at the position indicated by the green, dashed line in Figure 4.4. Both the tip apex position (upper panel) and the non-averaged lateral force on the cantilever (lower panel) are plotted.

cantilever oscillation at each tip apex jump results in very complex and erratic cantilever behaviour. On the other hand, during episodes in which the tip apex is localized in a certain lattice well, a well-defined, broad band is visible in the middle panel of Figure 4.4, which means that the oscillation of the cantilever is not disturbed.

The insight in the influence of a tip-apex jump on the cantilever motion brings us to a new level of understanding of single-asperity friction. First, as the cantilever is not damped significantly (in our calculations it is even completely undamped), the energy inserted into the complete 2-mass-2-spring system by the moving support, has to be dissipated exclusively via the tip-surface contact eventually. So all energy present in the cantilever oscillation will finally reach the friction contact, although energy can be stored in the cantilever motion temporarily. The coupling of the cantilever to the tip apex is rather weak ($m_{\mathrm{d}}/m_{\mathrm{cant}} < 10^{-10}$). Therefore, direct dissipation of the cantilever's kinetic energy via the resulting, forced motion of the tip apex is negligible, as can been recognized in the second panel of Figure 4.4, where the amplitude of the cantilever oscillation remains nearly constant between subsequent jumps of the tip apex. The only way for the cantilever to lose energy efficiently, is by a sudden loss of potential energy as the direct consequence of a sudden change in the equilibrium

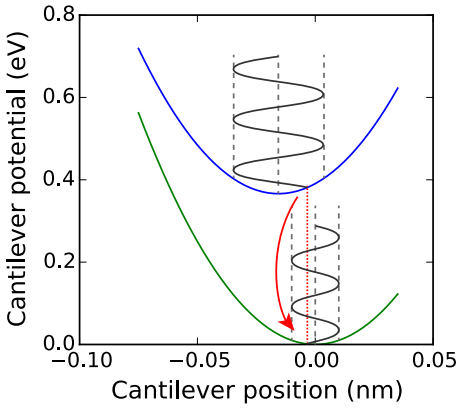

Figure 4.6: A schematic view of the change of the cantilever potential due to a jump of the tip apex. The situations before and after the jump are indicated by the blue and green curves respectively. The two curves indicate the full potential experienced by the cantilever, as a result of its connections to both the support and the tip apex. The oscillatory motion of the cantilever is indicated by the sine function. During the rapid jump of the dynamic tip apex, the position of the cantilever is not changed. The precise position and velocity of the cantilever at the moment of the tip apex jump determines its new amplitude and phase.

position of the cantilever. The equilibrium position of the cantilever is determined by the positions of the support and the tip apex (and their spring coefficients). The position of the support can be considered to remain unchanged on the timescale of a slip event. However, a jump of the tip apex from one lattice well to another takes place at a timescale characterized by the eigenfrequency of the tip apex, which is in the THz-regime. As a consequence, each time the tip apex jumps, both the equilibrium position of the cantilever and the potential energy stored in the tip-cantilever spring are changed. As the cantilever moves very slowly with respect to the tip apex, the cantilever experiences instantaneously a different force after a sudden jump of the tip apex. This results in abrupt changes of both the amplitude and phase of the cantilever oscillation. Basically, the position of the cantilever at the moment the tip-apex jumps, is crucial for its future motion. A schematic view of the change of the cantilever potential and its motion before and after a tip apex jump is shown in Figure 4.6. Note, that the change in potential energy of the cantilever goes hand in hand with an opposite change in kinetic energy of the tip apex, which is accelerated or decelerated due to the force exerted by the cantilever. This forms a highly efficient pathway for the exchange of energy between cantilever and tip apex, as is illustrated by the strong variations in the cantilever's oscillation amplitude in Figures 4.4, 4.5 and 4.6.

4.4.4 Slip duration, intermediate tip positions

Most of the highly time-resolved experiments presented in Reference [15] were performed on a KBr(100)-lattice. In order to check the influence of the substrate, we also performed numerical calculations using a lattice potential corresponding to the KBr(100)-lattice. The result of a calculation using a lattice corrugation of 0.45 eV (peak-peak) is shown in Figure 4.7. The scanning support of the cantilever was moved over 5 lattice constants, comparable to the calculations for graphite. The upper panel of Figure 4.7 shows the distribution of the x-coordinate of the tip apex as function of time. A pronounced difference with respect to the calculations performed on a graphite lattice, is the alternating long and short residence time of the tip apex in lattice wells. In the calculations shown in the upper panel, 11 locations are visible at which the tip apex resided (including the starting position). One might have expected to observe only 4-5 tip apex jumps, as the support moves over 5 lattice spacings. However, intermediate jumps are present. These are sideways jumps of the tip apex to the most easily accessible wells. In other words, the apex jumps not purely in the x-direction in which the motion of the support takes place, but it follows a minimum-

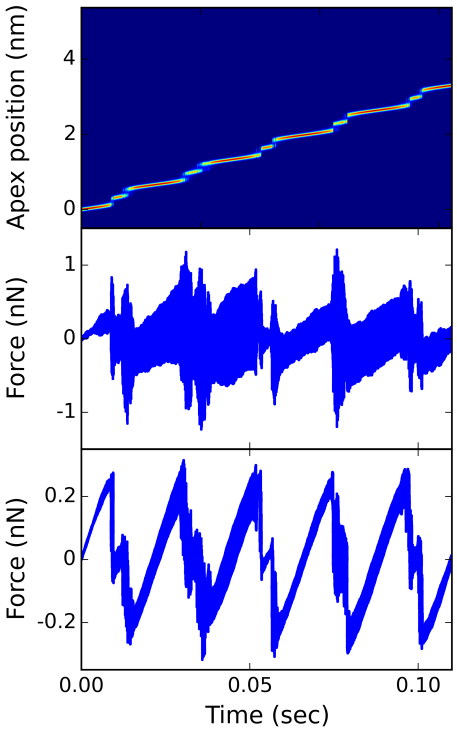

Figure 4.7: (Upper panel) Distribution of the x-coordinate of the tip-apex plotted as function of time. Each vertical column of pixels originates from one histogram. (Center panel) Unfiltered, 20 MHz data representing the lateral force on the cantilever. (Bottom panel) Lateral force data averaged in order to simulate experimental conditions (as applied in Reference [15]). The calculation was performed on a KBr(100)-lattice, using the following parameters: $U_0 = 0.45\,\mathrm{eV_{pp}}$, $m_{\mathrm{cant}} = 10^{-10}\,\mathrm{kg}$, $m_{\mathrm{d}} = 10^{-18}\,\mathrm{kg}$, $v_{\mathrm{supp}} = 30\,\mathrm{nm/sec}$, and $T = 298\,\mathrm{K}$.

energy zig-zag trajectory over the surface, in which it passes through other energy wells at intermediate x-coordinates. The y-motion of the tip apex, recorded in our calculations, supports this interpretation.

A detailed look at the tip apex behaviour on graphite, as shown in Figure 4.5, reveals that also in that case the tip performs jumps with a length of half a lattice distance in the x-direction. Also on graphite, the tip performs jumps in the sideways directions. However, the position of the tip apex in those sideways-positioned lattice wells is energetically not very favoured, which leads to negligibly short residence times of the tip apex in these positions.

The dynamic behaviour of the tip apex jumping between lattice wells results in a very specific behaviour of the cantilever deflection, especially after data-averaging. This can be seen most clearly in the lower panels in Figures 4.4 and 4.7. On the KBr(100)-lattice, the stable, intermediate positions of the tip apex result in an extra level in the lateral force curves. On graphite, the jumpiness of the tip apex shows up differently in the friction force data. After averaging of the tip apex x-position over many individual jumps, a gradual slope emerges. This is the result of the statistical average of the amount of time the tip resides in the discrete lattice wells. So the rapid dynamics of the tip apex, which jumps between well-defined, discrete positions is obscured in the experiment by the both the relatively slow cantilever and the subsequent data averaging.

In short, in the experiment, the slips may appear like very slow events, however, in reality, each individual slip duration is more or less identical (characterized by the eigenfrequency of the tip apex) and the apparent slip duration is a consequence data averaging carried out on the deflection signal of the 'slow' cantilever. This new insight explains most of the data observed in Reference [15] and yields a more fundamental interpretation of their experiments, based on the dynamic behaviour of the friction contact.

4.4.5 The Q-factor of the cantilever

In Section 3.3.4 the damping of the cantilever was described by its Q-factor. As we show in Appendix A, the Q-factor of the cantilever can be expressed as follows.

$$Q = \frac{1}{2D}\left(1+\frac{4\pi^2 U_0}{k_{\mathrm{d}}a^2}\right)^2\sqrt{\frac{m_{\mathrm{cant}}}{m_{\mathrm{d}}}\frac{k_{\mathrm{cant}}}{k_{\mathrm{d}}}} = \frac{1}{2D}\left(1+\frac{k_{\mathrm{TSI}}}{k_{\mathrm{d}}}\right)^2\sqrt{\frac{m_{\mathrm{cant}}}{m_{\mathrm{d}}}\frac{k_{\mathrm{cant}}}{k_{\mathrm{d}}}}. \tag{4.4}$$

In this equation, not only the influence of the connection of the cantilever to the support and to the dynamic mass, but also the influence of the

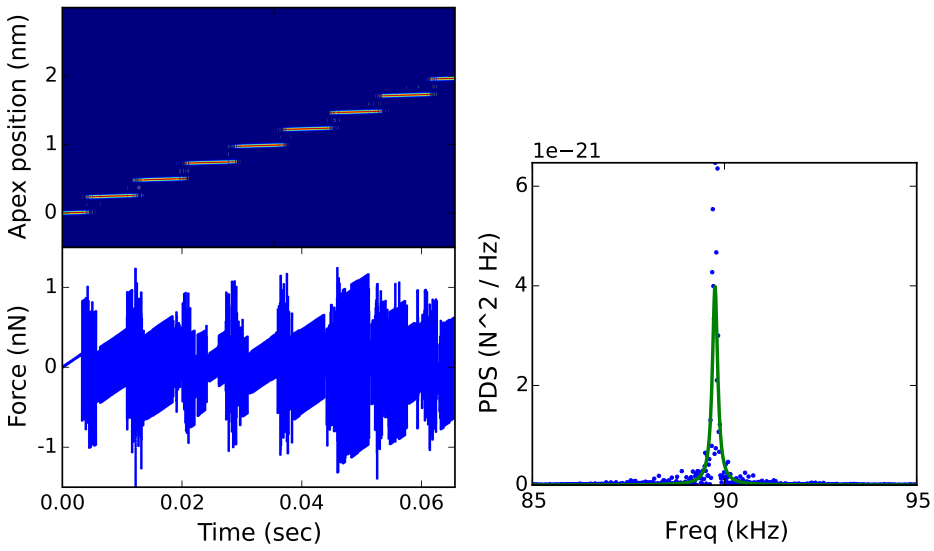

Figure 4.8: Result of a numerical calculation of a tip scanning over graphite at room temperature. (a) Distribution of the x-coordinate of the tip apex (top) and the non-averaged lateral force on the cantilever (bottom) during a typical SS-motion on graphite. (b) Fourier spectrum of the lateral force on the cantilever. The estimation of the Q-factor is indicated by the green fit, which is characterised by the following parameters: $FWHM = 83.1\,\mathrm{Hz}$, $Center = 89.8\,\mathrm{kHz}$, $Q = 540$.

tip-substrate interaction is taken into account.

The Q-factor of the cantilever is known to decrease many orders of magnitude when the tip is brought in contact with a substrate, although the origin of this effect is not fully understood yet [15]. Our numerical calculations present a suitable tool to investigate the effect of the tip-substrate interaction on the Q-factor of the cantilever. First, a calculation was done in which a typical FFM experiment was simulated. The cantilever and tip were dragged by the support moving at a velocity of 30 nm/sec over the graphene lattice potential with a corrugation of 0.4 eV, at room temperature. The Q-factor was determined by a Fast Fourier Transformation (FFT) and found to be approximately 540, see Figure 4.8. Second, a situation was created that was intended to realize a 'delocalized' tip that is jumping forward and backward between two lattice wells. To realise this, the support was fixed at a position just in between two lattice wells in the tip-substrate interaction potential, maximizing the enharmonic contribution of the inter-

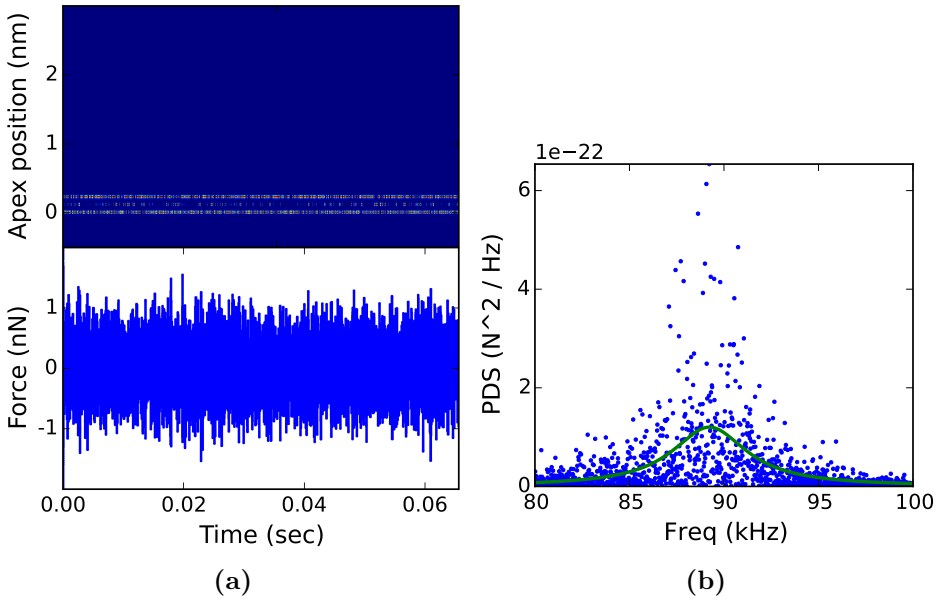

(a) **(b)**

Figure 4.9: Result of a numerical calculation at room temperature of a tip-cantilever system, while the support is positioned right in between two minima, i.e. above a local maximum, of the interaction potential between the tip apex and the graphite substrate. (a) Distribution of the x-coordinate of the tip apex (top) and the non-averaged lateral force on the cantilever (bottom) during a typical SS-motion on graphite. (b) Fourier spectrum of the lateral force on the cantilever. The estimation of the Q-factor is indicated by the green fit, which is characterised by the following parameters: $FWHM = 2.41\,\mathrm{kHz}$, $Center = 89.2\,\mathrm{kHz}$, $Q = 18.5$.

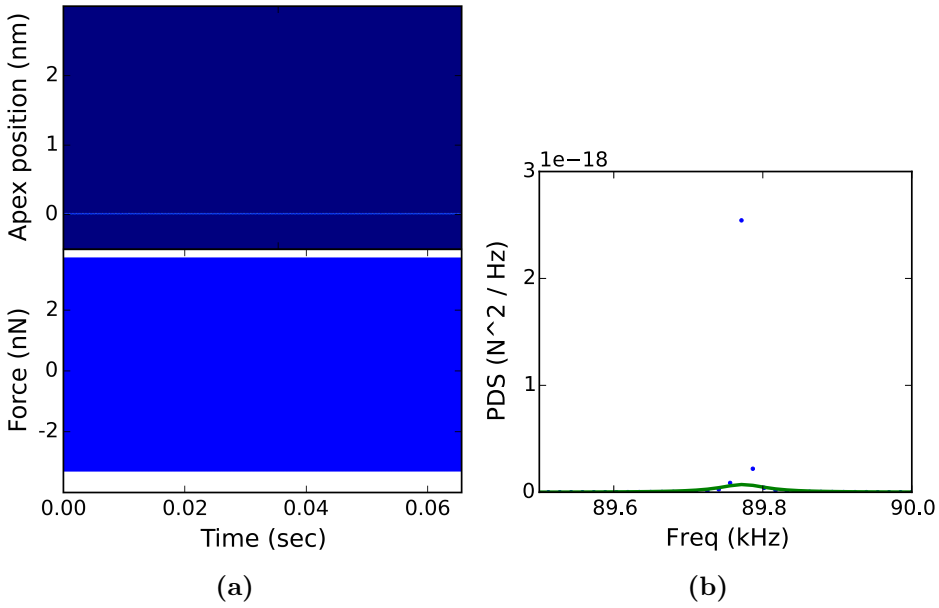

(a) **(b)**

Figure 4.10: Result of a numerical calculation of a tip-cantilever system, while the support is positioned right in between two minima, i.e. above a local maximum, of the interaction potential between the tip apex and the graphite substrate. The temperature wat set to 0 K in order to prevent thermally activated jumps of the tip apex. (a) Distribution of the x-coordinate of the tip apex (top) and the non-averaged lateral force on the cantilever (bottom) during a typical SS-motion on graphite. (b) Fourier spectrum of the lateral force on the cantilever. The estimation of the Q-factor is indicated by the green fit, which is characterised by the following parameters: $FWHM = 38.5\,\mathrm{Hz}$, $Center = 89.8\,\mathrm{kHz}$, $Q = 1170$.

action potential. The thermal fluctuations cause the tip to jump between the minima in the interaction potential many times, as can be seen in the results of the calculations that are presented in Figure 4.9. The Q-factor of the lateral force signal from the cantilever has dropped significantly to a value of 18.5. In order to verify that thermal fluctuations have been solely responsible for this strong reduction of the Q-factor, we have repeated the calculation for precisely the same configuration, i.e. with the support positioned precisely between two neighbouring potential wells, but now at zero temperature. As can be seen in Figure 4.10, the absence of fluctuations resulted in a very 'localized' tip. The Q-factor has increased to a value of at least 1170. In fact, this value should be regarded as a lower estimate of the Q-factor, as a result of the finite resolution of the calculation.

These numerical calculations reveal a dramatic impact of the tip-substrate dynamics on the measured Q-factor. As demonstrated in Figures 4.8-4.10, the mere presence of the lattice does not explain the deterioration of the Q-factor. In Section 4.4.3 we demonstrated that a delocalized tip apex that is jumping forward and backward, has a major impact on the amplitude and the phase of the oscillating motion of the cantilever. As a direct result, the cantilever motion can no longer be described properly by a single resonance frequency and the FFT acquires a significant width, as is illustrated dramatically in Figure 4.9. The impact of this noise on the Q-factor is in the order of several orders of magnitude. Summarizing we can state that the Q-factor is affected significantly by the dynamics of the tip apex.

Our findings are supported fully by the experimental results presented in Reference [15]. In that report, it can be recognized that the 'noisy' FFT-spectrum measured using a sharp tip on an $Al_2O_3(0001)$-substrate is fully consistent with the analysis and interpretation presented here. In addition, the spectra reported in Reference [15] that are recorded using micrometer-scale spherical tips do not exhibit the discussed 'noise', which is not a surprise as these tips are not expected to create a single-asperity contact with the substrate. As a consequence, the recorded lateral forces originate from an averaged behaviour of all individual nanocontacts of the blunt tip with the substrate.

Using the interpretation presented here, both the qualitative nature of the lateral force spectra and the quantitative behaviour of the Q-factor is explained. The origin of the behaviour of the measured cantilever deflection is rooted in the extremely dynamic behaviour of the tip apex. Although the cantilever is much heavier than the tip apex, every single high-frequency slip of the tip apex affects the cantilever motion, resulting in a significant

impact on the Q-factor of the cantilever.

4.5 Summarizing conclusions

Numerical calculations using the refined 2-mass-2-spring model resulted in friction force maps that contained a limited regime in which atomic periodicities are clearly observed. This regime is characterised by a specific ratio between the number of atoms present in the contact and in the dynamic mass. When this ratio led to a critically damped tip apex, regular SS-patterns were observed. In other scenarios, either the underdamped tip apex led to multiple slips or the overdamped tip apex resulted in a stochastic-type of stick slip.

Our numerical model allowed us to zoom in on the motion of the tip apex and on the reaction of the cantilever on slip events of the tip apex. Based on the experimental support of the results of our calculations, we revealed the behaviour of the tip apex of a friction contact. The typical observations of the lateral deflection of the cantilever was explained and further insight in special behaviour of the tip apex was achieved.

Also, we concentrated on the Q-factor of the cantilever. The absence of explicit damping on the cantilever and the marginal damping of the cantilever via the small tip apex could not explain the drop in the A-factor that is typically reported in literature. We showed that the SS-behaviour of the tip apex as a significant influence on the determined Q-factor of the cantilever.

Based on our theoretical model of a friction contact and on the calculational results, we constructed a friction 'phase' diagram. As most tips used in AFM- and FFM-experiments have geometries that make the tip apex naturally critically damped, regular SS-motion is readily observed. Deliberate construction of asperities with a geometry that would lead to low friction contacts, opens a way to predict and tune the friction of maybe even macroscopic surfaces.